PAPER

Check for updates

Designing hydrophobic, anti-soiling coatings for solar module cover glass: degradation mechanisms to avoid

Luke O. Jones, [iD] *[ab] Adam M. Law, [iD] [a] Gary W. Critchlow[b] and John M. Walls[a]

In this paper, we identify the degradation mechanisms occurring with these coatings, in this way, we can identify more suitable coatings whose chemistry avoids these degradation pathways. Two such coating technologies used in other applications are perfluoropolyether (PFPE) and 1*H*,1*H*,2*H*,2*H*-perfluorodecyl-triethoxysilane (FAS-17). These polymeric hydrophobic coatings were deposited on soda–lime glass substrates and tested for 1000 hours in an accelerated UV exposure test and a damp heat test in a laboratory environment. After 1000 hours of UV exposure, the coatings experienced degradation with the PFPE coating degrading *via* β scission of the central ether bond whilst the FAS-17 underwent photo-oxidation at the C–Si bond. During damp heat testing the PFPE degraded by hydrolysis at the central ether bond whilst FAS-17 exhibited resistance to hydrolysis. The chemical mechanisms responsible for the degradation are identified. The objective is to discover alternative transparent hydrophobic materials that do not contain the same weaknesses in their chemical structure.

1. Introduction

The cost of photovoltaic (PV) generated electricity has reduced substantially over the past decade. When comparing the levelized cost of electricity (LCOE) with other methods of electricity generation, both renewable and non-renewable, solar PV is the cheapest form of electricity generation worldwide.[1] Cost reductions have been achieved largely by improving the efficiency and reliability of solar modules. However, solar asset managers are faced with expensive maintenance issues that affect operational efficiency, and these issues now deserve increased research effort.[2]

A serious concern for solar utility management is the issue of soiling on the cover glass surfaces of solar panels.[3–5] Soiling is a complex phenomenon that affects the power generation of solar panels during their lifetime. Dust, dirt, debris, and biological matter can adhere to the surface of the cover glass and attenuate the light transmitted into the PV absorber. The reduction of transmitted light reduces the current density and decreases power output.[6] Soiling losses vary depending on the geographical location of the solar site from 0.01–0.1%/day in Europe[7] and North America,[8] between 0.2–0.4%/day in humid

climates such as South Asia,[9] and as high as 1–2%/day in arid climates such as East Asia, and the Middle East and North Africa (MENA).[8]

1.1. Soiling mitigation of the cover glass

The propensity of soiling on solar module cover glass can be attributed to the high surface energy of the cover glass, this has been highlighted by several authors.[10–12] A previous study compared particle adhesion for soda–lime glass, porous SiO_2 single layer, and multilayer ARC which all exhibited hydrophilic properties against a hydrophobic polymer, anti-soiling coating. The study utilized Arizona test dust in an in-house dust-dew-dry cycle test; which demonstrated that dust particles cement to the surface of the hydrophilic materials at a higher rate than the hydrophobic materials. The hydrophilic materials exhibited a reduction in optical light transmittance of the uncoated cover glass by nearly 50% and the porous SiO_2 coated glass by 100% compared to the hydrophobic polymer's 22%.[13]

Hydrophobic, anti-soiling strategies can be used to reduce the adherence of soiling to the surface, and/or promote removal of the debris once it has interacted with the cover glass. Similar strategies have been employed in other fields such as with ophthalmic spectacle lenses with an anti-reflective coating. The concept of using hydrophobic coatings to reduce soiling and to make modules easier to clean has already been demonstrated extensively in the field of PV.[14–18]

The rainfall and wind exposure additionally aid the removal of soiling particles for low surface energy coatings, as noted by

[a] *Centre for Renewable Energy Systems Technology (CREST), Wolfson School of Mechanical, Electrical and Manufacturing Engineering, Loughborough University, Loughborough, Leicestershire LE11 3TU, UK. E-mail: l.jones8@lboro.ac.uk*

[b] *Department of Materials, Loughborough University, Loughborough, Leicestershire LE11 3TU, UK*

Huang et al.[15] The flow rate of wind (and by extension rain) provides the kinetic energy to dislodge soiling particles from the surface of the PV module cover glass. This was found to be applicable to hydrophobic (WCA > 90°) coatings as well as superhydrophobic coatings (WCA > 150°) which performed the best in testing, typically exhibiting efficiency losses less than 1% compared to uncoated glass which exhibited efficiency losses of up to 6.5%. Superhydrophobic coatings were found to perform the best, followed by hydrophobic coatings, then hydrophilic coatings. It was found that superhydrophilic coatings (WCA < 10°) were highly detrimental to the efficiency of PV modules as the high surface energy caused particles to adhere strongly to the surface, resisting the dislodging effects of the wind.[15–18]

1.2. Hydrophobic coating degradation

Common polymers used in commercial hydrophobic coatings include the fluoropolymers fluoroalkylsilane (FAS),[19–21] fluorinated ethylene propylene (FEP),[22,23] polyfluoropolyether (PFPE),[24,25] and non-fluorinated variants such as polydimethylsilane (PDMS)[13,20,21,26] and polymethyl methacrylate (PMMA).[20] When used as an anti-soiling coating for solar PV, these coatings can achieve high optical transmittance, over 90%, with hydrophobic water contact angles of 110° typically for PDMS and PMMA, and up to 130° for the fluoropolymers. However, although the commercial hydrophobic coatings showed proof of principle for anti-soiling on PV modules, the benefits were not long lived.

A study conducted by Lisco et al.[18] on coatings using scanning electron microscopy (SEM) showed the damage caused to 3 types of anti-soiling coating chemistries (2 fluoropolymers and 1 non-fluorinated polysiloxane). When the coatings were subjected to 1000 hours of DH and UV accelerated ageing, each of the three coatings exhibited loss of hydrophobicity, blistering, and coating thinning. Additionally, the outdoor experiments conducted by Oehler et al.[27] reported that when exposed to outdoor environments, further abrasion damage is observed using SEM imaging either from environmental particles/debris, or from coatings that contain functionalised nanoparticles (FNPs) detaching from the coating mixture and abrading along the surface during cleaning cycles. The mechanical damage caused by abrasion constitutes the physical removal of hydrophobic material used for anti-soiling purposes.

Chemical degradation may also be a factor reducing the effective lifetime of an anti-soiling coating. Organic coatings can react to temperature, humidity,[28] and UV irradiance[29] in the atmosphere which alters the chemical architecture of the coating chemistry, leading to loss of hydrophobic functional groups.[25,26] During prolonged exposure to UV radiation, photo-oxidation can occur in organic polymers causing the breakdown of backbone chains. This has been reported in studies of encapsulant materials such as ethylene-vinyl acetate (EVA).[30] However, this can also occur in other polymers as reported in an extensive review by Yousif and Haddad[31] and a study on polymer UV degradation products by Sørensen et al.[32] Polymers such as polystyrene (PS), polyester (PET), polyamide (PA), etc. undergo photo-oxidation, due to UV free radical species and decompose into monomers/oligomers via chain scission. This process occurs due to factors such as UV intensity, oxygen content in air, ionization, heat, and both internal and external chemical factors.[33]

The presence of water is additionally problematic for Solar PV. Coastal PV installations, floating PV, and sites in locations that feature plentiful rainfall must take into consideration how hydrolysis can impact the degradation of a polymeric anti-soiling coating. Hydrolysis of carbon chains acts similarly to degradation caused by UV free radicalization, where chain scission occurs due to the reaction of polar water molecules (nucleophiles) with the electrophilic polar species of an anti-soiling coating, typically functional groups within the polymer chain such as ether (C–O–C), carbonyl (C=O), or carboxyl bonds (COOH) where the carbon is partially charged (δ^+).[34] While degradation via hydrolysis is repelled in hydrophobic coatings containing predominantly fluorocarbon bonds,[35] weaknesses within the chain, such as ether groups found in perfluoropolyethers (PFPE), unprotected δ+ carbons in the backbone chain structure,[36] and/or susceptible contaminant species left over from chemical production[25] can be targeted by nucleophilic species leading to degradation.

Whilst it has already been established that the fluoropolymer hydrophobic coatings degrade through the loss of fluorine on outdoor exposure,[18,25,27] there is a fundamental gap in understanding the mechanisms causing the loss of anti-soiling properties. Little research has been focused on long term or accelerated degradation studies of anti-soiling, hydrophobic coatings for use on PV modules. The precise degradation mechanisms have not been explored.

In this study the long-term environmental durability of fluorinated anti-soiling coatings have been tested to determine the degradation mechanisms when exposed to individual accelerated degradation methods that may be experienced during outdoor conditions during operation. The optical and hydrophobic performance has been correlated with surface analysis using high resolution X-ray photoelectron spectroscopy (XPS) to obtain evidence of the initiation and propagation of failure modes in the degrading coatings. This work aims to understand these degradation mechanisms, which will assist in the development of high performance, low surface energy, and weather resistant anti-soiling coatings with durability suited to the extreme demands of PV modules.

2. Experimental

2.1. Materials & sample preparation

Hydrophobic polymers, used as an anti-soiling coating, were selected to explore the degradation mechanisms caused by UV and DH accelerated ageing. Clear, ISO 8037-1 soda–lime glass slides (purchased from Fisher) were cleaned coating using a multi-step cleaning process. The glass was first rinsed by hand using a gentle surfactant wash. Deionised water was then used

to remove any leftover surfactant, and the samples were then placed in an ultrasonicated bath using using 99.9% acetone for 30 minutes at 40 °C. The glass slides were then rinsed in deionized water and dried using compress air. A final preparation step of UV-ozone surface cleaning for 20 minutes using an Ossila UV Ozone Cleaner was performed immediately before coating to maximise surface energy. Several glass slides were then sent to an ophthalmic company for the application of the first hydrophobic coating application.

The first coating was a commercially available perfluoropolyether (PFPE) coating and used in the ophthalmic industry. It was applied *via* dip coating from the coating manufacture using a proprietary technique. The second coating was a research based fluoroalkylsilane, 1*H*,1*H*,2*H*,2*H*-perfluorodecyltriethoxysilane (FAS-17) solution applied *via* dip coating. The cleaned glass slides were dipped in a solution prepared of 98% active ingredient FAS-17 solution (purchased from Sigma-Alderich), which was diluted in 99.8% methanol in a 2 : 98 weight ratio. The combined solution was stirred continuously for 60 minutes for homogeneous mixture. The glass slide was then submerged in the combined solution at a rate of 1 mm s^{-1} for both submersion and extraction. The entire dip coating time took 140 s. After extraction the coated slide was left to hang for residue solution to drip off. After coating application, the surfaces were left to cure in ambient temperature overnight until the solvent had dispersed and a hard coating remained.

on the samples at intervals of 250-hours from as-deposited to 1000 hours of exposure.

2.4. Analysis methods

Surface chemical analysis was conducted using X-ray photoelectron spectroscopy (XPS). All spectra were recorded using a Thermo Scientific K-Alpha XPS with a monochromated Aluminium Kα source. The sample surface was characterised using survey scans and high-resolution scans obtained with the following parameters: Surveys were measured using 100 eV pass energy, 1 eV step size, 10 ms dwell time averaged over 10 Scans. High-resolution scans were measured using 25 eV pass energy, 0.1 eV step size, 50 ms dwell time averaged over 5 scans for each element of interest. All results were charge corrected to carbon C 1s at 284.8 eV.

Coating optical performance was measure using transmission and reflection measurements taken across a wavelength range of 200–1200 nm using a Varian Cary5000 UV-VIS spectrophotometer with an integrating sphere attachment. The scan rate was set at 600 nm min^{-1} with a step size of 1 nm. Weighted average transmission (WAT) values were used to spectrally-weight the value of optical transmittance considering the variation in photon flux of the AM1.5g solar spectrum, across the measured wavelength range of interest. Using WAT provides a single value of reflectance that is applicable for solar applications and can be calculated using eqn (1). Where Φ is the photon flux and T is the percent transmittance at each given

PFPE

FAS-17
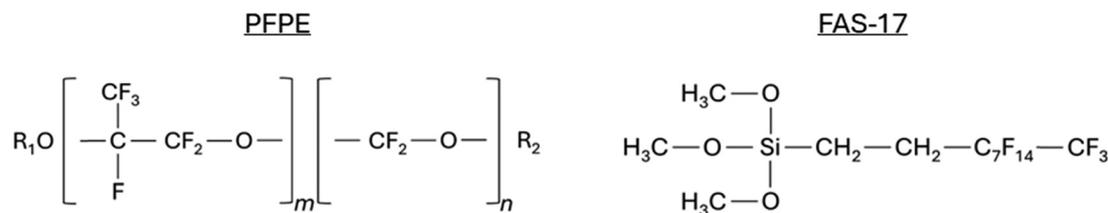
2.2. UV accelerated exposure

All samples were subjected to an ultraviolet (UV) exposure test for up to 1000 hours. The UV exposure test was conducted using a QUV Accelerated Weathering Tester at wavelengths between 280 nm and 400 nm, and a minimum of 15 kWh m^{-2} of UV light, with a 3% to 10% of the total energy in the UVB light range (in accordance with BS EN 61215-2). Intermediate measurements were made to monitor the effects of UV on the samples at intervals of 250-hours from as-deposited to 1000 hours of exposure.

2.3. DH accelerated exposure

All were subjected to a DH exposure test for up to 1000 hours. The DH exposure test was conducted using a Delta 190H Temperature/Humidity Test Chambers at 85 °C and 85% relative humidity (RH) (in accordance with BS EN 61215-2). Intermediate measurements were made to monitor the effects of DH

wavelength, λ. The calculations were performed using a custom Matlab script.

$$\text{WAT}(\lambda_{\min}, \lambda_{\max}) = \int_{\lambda_{\min}}^{\lambda_{\max}} \frac{\Phi \cdot T}{T} \text{d}\lambda \qquad (1)$$

Contact angle measurements were made using the static sessile drop method with a Dataphysics OCA20 contact angle measurement system and a water droplet volume of 3 µl. The measurement was carried out six times for each sample and the uncertainty was evaluated as the standard deviation (σ) of the six measurements.

3. Results & discussion

3.1. Coating characterisation

After deposition the coatings increased the water contact angle (WCA) from hydrophilic to a hydrophobic state. The high WCA indicates the low surface energy of the coating materials.
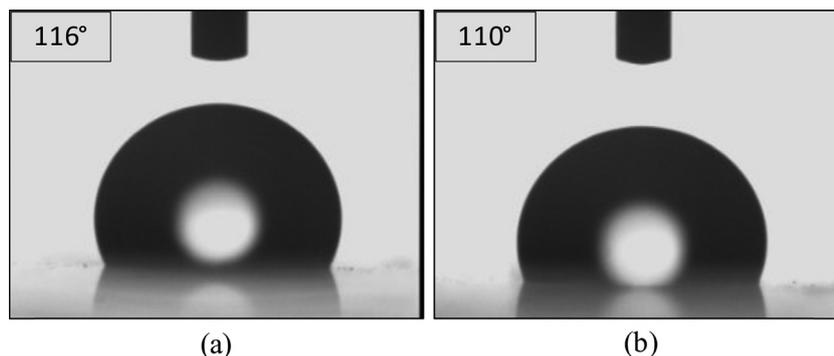
Fig. 1 (a) PFPE ophthalmic hydrophobic coating deposited on glass exhibiting a water contact angle of 116°. (b) FAS-17 hydrophobic coating deposited on glass exhibiting a water contact angle of 110°.
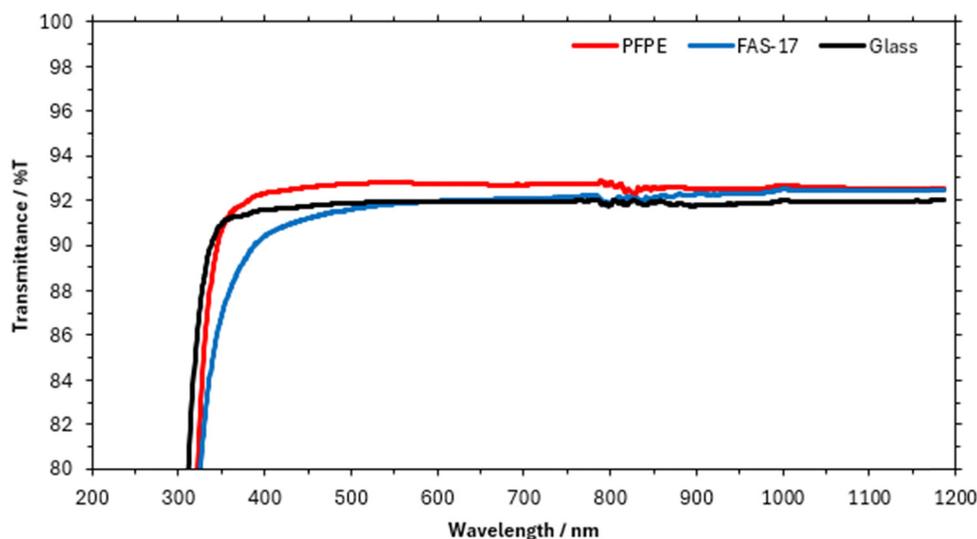

Fig. 2 Optical transmittance of hydrophobic, anti-soiling coatings deposited on soda–lime glass substrate compared to a soda–lime glass control. The feature between 800 and 900 nm is due to detector crossover during data collection.

The PFPE, Fig. 1(a), and FAS-17, Fig. 1(b), coating increased the WCA of the glass substrate from $14.2 \pm 1.9°$ to $117.0 \pm 1.0°$ and $112.5 \pm 1.7°$ respectively, indicating the effectiveness of these materials as a hydrophobic coating. Additionally, an added benefit of using these polymers as a coating is their effect on the optical properties of the cover glass. The polymer coatings have a higher transmittance, Fig. 2, than glass due to their lower refractive indices, $n = 1.29$ for PFPE, and 1.34 for FAS-17 at 550 nm. The lower refractive index of the polymer coatings increases internal reflectance, thereby reducing emitted reflectance of light between the polymer coating and air. This reduction in reflectance directly correlates to an increase in total light transmitted through the coated glass which would be proportional to increased power generation in a PV module. The coatings increase the weighted average transmission (WAT) compared to the glass substrate, increasing the WAT from 91.9 T% for glass up to 92.6 T% and 92.4 T% for PFPE and FAS-17, respectively. The increase in optical transmittance would directly correlate to an increase in short circuit current (J_{sc}) as more light would be incident on the PV absorber.

XPS was used to identify the surface elements. Initial observation using survey scans revealed the main elements found in each of the coatings were C, F, Si, and O of varying ratios. Analysing the C 1s high resolution (HR) spectra, we can see both characteristic peaks identifying the difference in polymeric structure between coatings. PFPE has peaks, Fig. 3, at 284.8 eV for C–C/C–H, 286.2 eV for C–O, 291.4 eV for OCF, 293.1 eV for OCF_2, and 294.6 eV for OCF_3, which are typical peak binding energy values for

PFPE lubricants,[37] additionally, the presence of OCF and OCF_3 peaks indicate that the type of PFPE lubricant used contains a side chain structure $(–CF(CF_3)–CF_2–O–)_m$ and terminates in an OCF_3 functional group. The C–O bond is due to the central ether bond (C–O–C) in the polymer structure as opposed to surface contaminants. FAS-17 features similar peaks to PFPE however the C–O signal is larger due to the siloxane group at the end of the polymer chain. FAS-17 exhibits prominent peaks at (VI) 291.4 eV for CF_2 and (VII) 293.7 eV for CF_3 due to the absence of O atoms in its central chain. The CF_2 signal is greater due to the long C_8F_{17} chain comprised of mostly CF_2
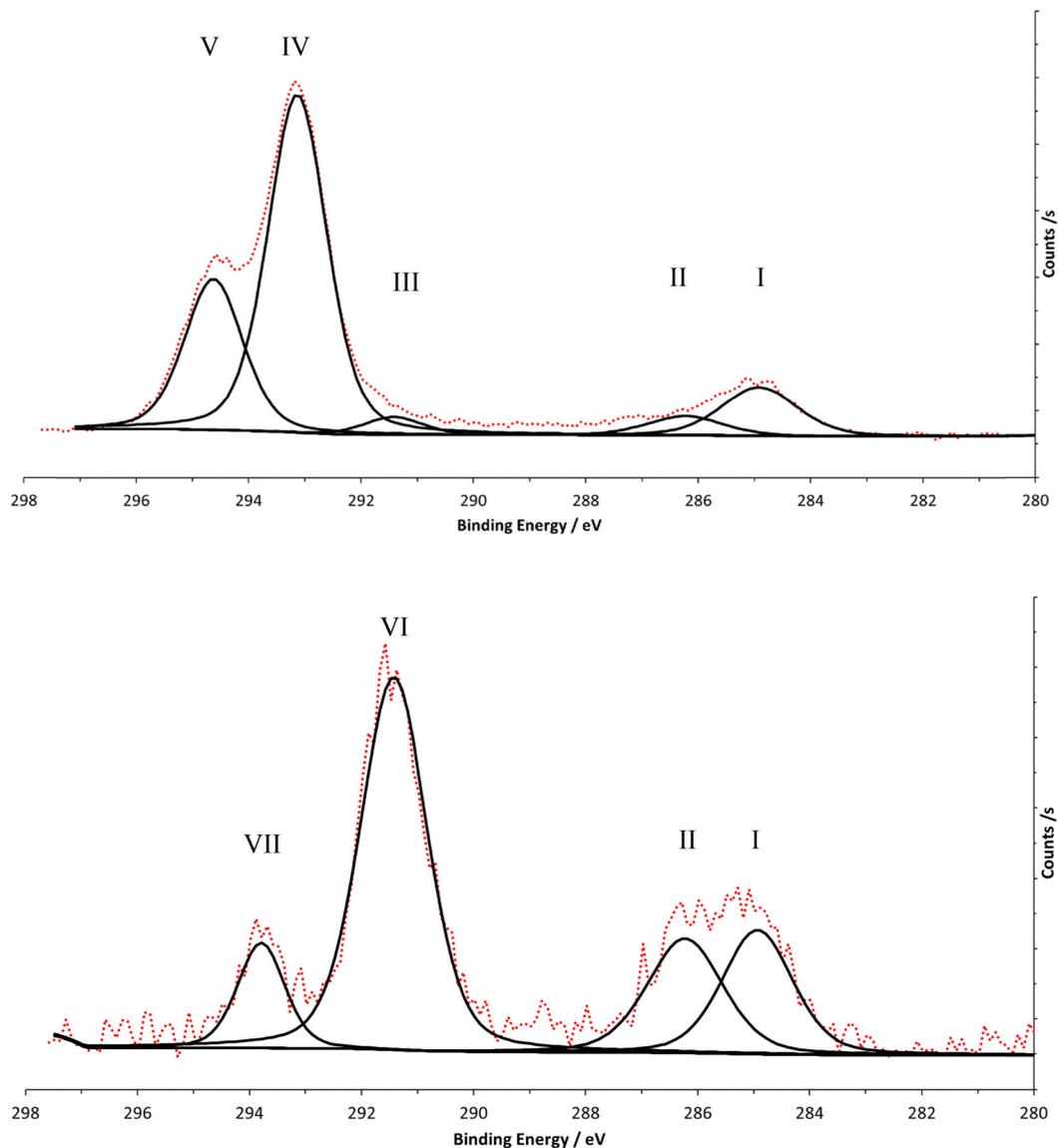
Fig. 3 C 1s high resolution XPS spectra for (top) PFPE coating and (bottom) FAS–17 coating.

repeating units. The FAS-17n coating exhibited similar peak position and peak intensities as FAS-17, however it had a stronger SiO_2 signal at 102.8 eV due to the presence of the nanoparticles increasing the surface signal. Alterations of these bond peak positions and atomic % ratio will indicate the degradation mechanisms during accelerated weathering exposure.

3.2. UV accelerated exposure

After 1000 hours of exposure in the accelerated UV weathering chamber the coatings exhibited performance losses for both optical and hydrophobic performance, Fig. 4. The PFPE coating started with the highest WAT at 92.6 T%, however, by 250 hours, the transmittance had decreased by an absolute $\sim 1.0\%$, and by 1000 hours, it had decreased by a total $\sim 1.8\%$ absolute loss finishing at a WAT of 90.8 T%. The FAS-17 coating also showed an initial decrease of WAT after 250 hours,

reducing from 92.4 T% to 91.8 T%, however the WAT remained constant until the 1000-hour testing had terminated. The glass control WAT decreased by <2 T% from 91.9 T% to 90.3 T%. Despite the stable optical performance of the FAS-17 coating, it performed the poorest during the hydrophobicity testing. The FAS-17 coating WCA reduced from 112.5° to 66.8° after 750 hours and did not recover, losing its hydrophobic properties and becoming hydrophilic. Conversely, the PFPE coating's WCA remained stable during testing decreasing from 117.0° to 111.0° after 1000 hours.

The PFPE coating exhibited the greatest optical degradation during UV exposure however it still retained its hydrophobic properties. This indicates that the PFPE coating retained the majority of its non-polar functional groups, but during degradation, intermediate species are formed that effect the optical properties of the coating. Conversely, the FAS-17 coating maintains high optical properties but the immediate decrease
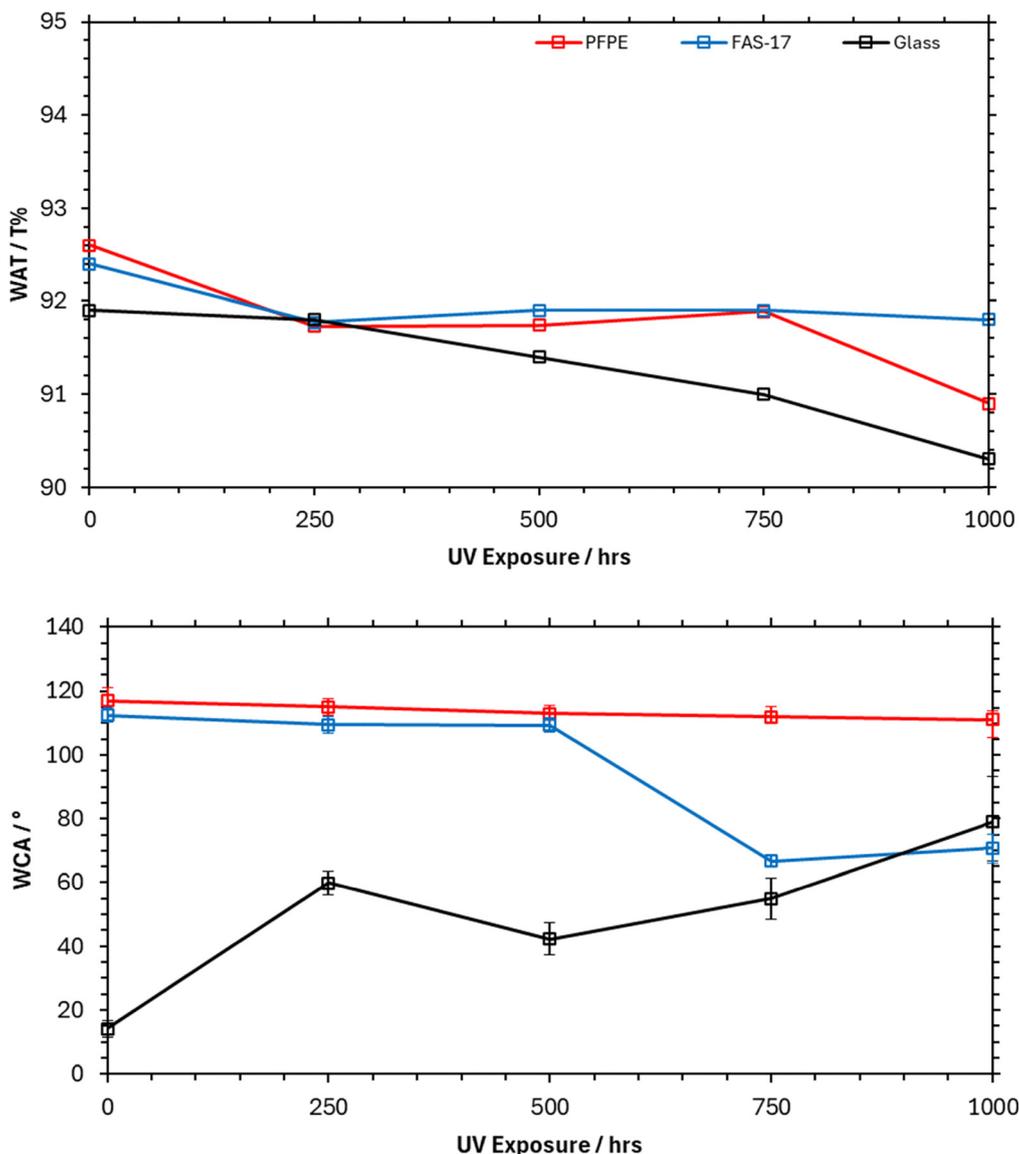
Fig. 4 (top) Weighted average transmission and (bottom) water contact angle of hydrophobic, anti-soiling coatings after 1000 hours of accelerated UV exposure compared to a soda–lime glass control.

in hydrophobicity indicates complete removal of the non-polar functional groups from the sample surface and no intermediate species forming that would impact the optical performance. This is supported by the XPS spectra of C 1s and F 1s for both materials, where the PFPE maintained high F 1s content, decreasing from 42.2 at% to 36.0 at% over 1000 hours compared to the FAS-17 coating which saw a reduction from 47.1 at% to 2.4 at% after 1000 hours.

The decrease in surface energy of the glass control is due to the surface contaminated by organic material during testing as evident by the visual inspection and XPS surface analysis. XPS reveals the C content on the surface of the glass increased from 7.6 at% to 68.4 at%, predominantly as C–C/C–H peaks at 284.8 eV, from 0 to 1000 hours. Hydrocarbons are non-polar species and would be responsible for the increase in WCA of the glass.

3.2.1. PFPE degradation mechanisms. Due to the chemical stability of fluoropolymers, there is a limit to the mechanisms of degradation of the C–F bonds due to the large difference in electronegativity between C and F (2.55 and 3.98 respectively), short bond length and high radiation energy required to break the bond.[38] Therefore, for the PFPE coating to break down under UV exposure, areas that are more susceptible to electronegative radicals are targeted such as the C–C bond and C–O bonds found within the central carbon chain of the polymer.[39]

Based on the results of the XPS analysis, Fig. 5a, and literature,[39–41] the likely mechanism of degradation would be due to photo-oxidative degradation of the central ether (C–O–C) bonds of the PFPE coating. Two susceptible secondary carbons can be found in the polymer chain, α and β, due to the presence of the neighbouring O atom adversely affecting the electron
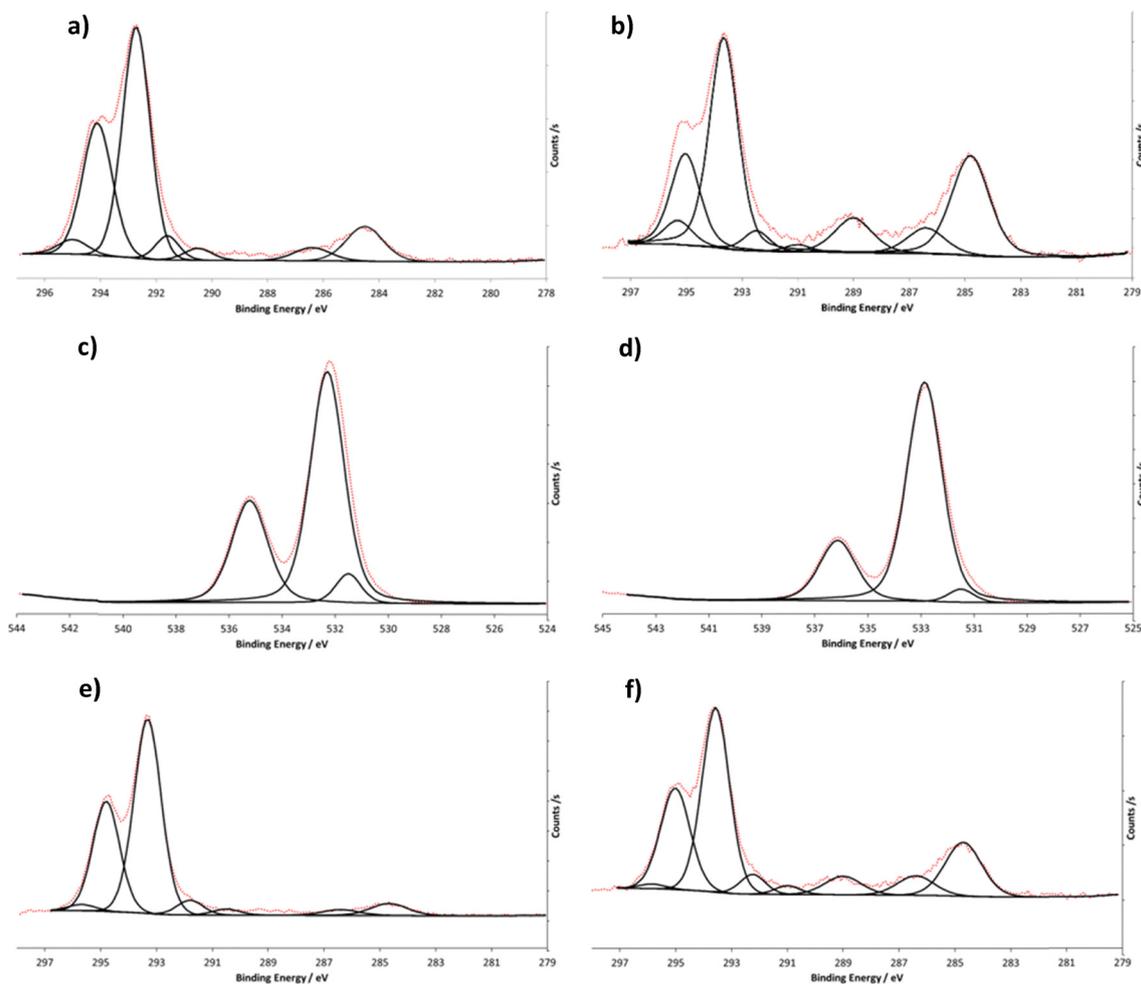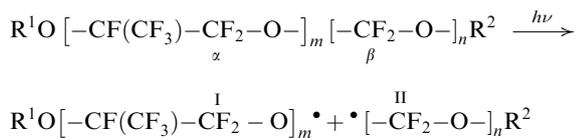
Fig. 5 High resolution XPS spectra for PFPE coated samples over 1000 hours of UV exposure. (a) C 1s spectra after deposition, (b) C 1s spectra after 1000 hours, (c) O 1s spectra after deposition, (d) O1s spectra after 1000 hours, (e) C 1s spectra 500 hours, (f) C 1s spectra after 750 hours.
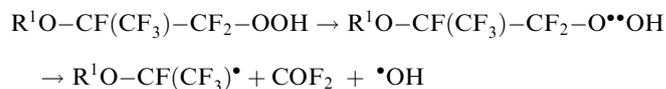
withdrawing effect of the CF_x bonds. These carbon atoms can be targeted by radiative energy ($h\nu$) causing initial chain scission of the polymer chain generating fluoroalkoxy radicals.

$$R^1O\left[-CF(CF_3)-\underset{\alpha}{CF_2}-O-\right]_m\left[-\underset{\beta}{CF_2}-O-\right]_nR^2 \xrightarrow{h\nu}$$

$$R^1O\left[-CF(CF_3)-\overset{I}{CF_2}-O\right]_m^\bullet + {}^\bullet\left[\overset{II}{-CF_2-O-}\right]_nR^2$$

The scission of the PFPE chain will results in a radical species ending with a free electron situated on oxygen atom (I) or the carbon atom (II). The presence of O_2 and H_2O in the atmosphere will interact the radical species to form hydroperoxide species (–OOH). This process can be seen to occur between 500 hours and 750 hours as the signal from the C–O peak at 286.1 eV increases by 100%, Fig. 5e and f.

$$R^1O-CF(CF_3)-CF_2-O^\bullet + {}^\bullet CF_2-O-R^2 \xrightarrow{O_2+H_2O}$$
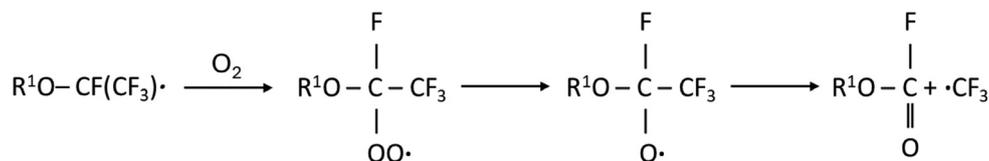
$$R^1O-CF(CF_3)-CF_2-OOH + HOOCF_2-O-R^2$$
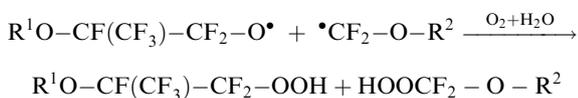
The hydroperoxide species are regularly decomposed thermally or photochemically. Scission of the O–O bond of the hydroperoxide produces fluoroalkoxy radicals and 2 hydroxyl radicals. The fluoroalkoxy radical will undergo β-scission and homolysis of the C–C bond of the neighbouring carbon resulting in a fluoroalkyl radical and carbonyl fluoride (COF_2).

$$R^1O-CF(CF_3)-CF_2-OOH \rightarrow R^1O-CF(CF_3)-CF_2-O^{\bullet\bullet}OH$$

$$\rightarrow R^1O-CF(CF_3)^\bullet + COF_2 + {}^\bullet OH$$

The resulting β-scission results in loss of CF_2 species as evidenced by the drop in CF_2 and COF_2 peaks in the XPS at 293 eV and 294.5 eV respectively. By 1000 hours of UV exposure the COF_2 signal has reduced by 40% and a peak at 288.6 eV is present, Fig. 5b, which indicates the presence of carbonyl bonds (C=O). The presence of carbonyl bonds can only be attributed to further photo-oxidation of the fluoroalkyl radical to produce a formate, and trifluoromethyl radical.
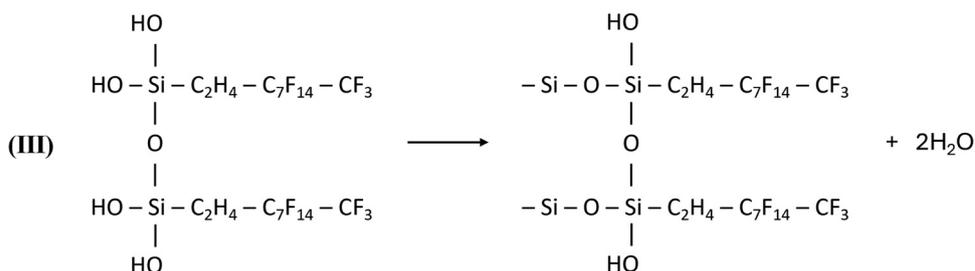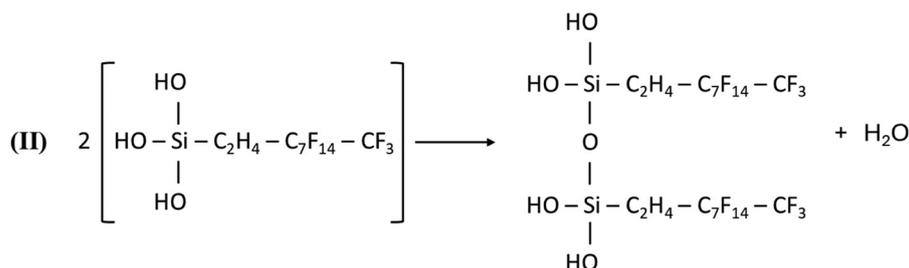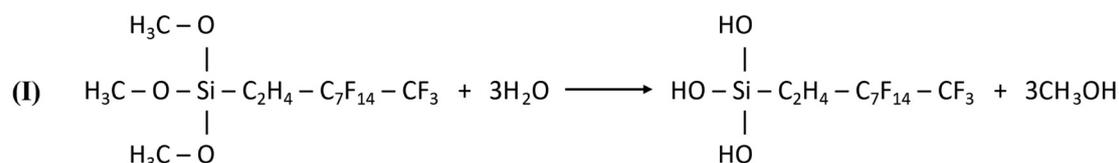
$$R^1O-CF(CF_3)\cdot \xrightarrow{O_2} R^1O-\underset{\underset{OO\cdot}{|}}{\overset{\overset{F}{|}}{C}}-CF_3 \longrightarrow R^1O-\underset{\underset{O\cdot}{|}}{\overset{\overset{F}{|}}{C}}-CF_3 \longrightarrow R^1O-\underset{\underset{O}{\|}}{\overset{\overset{F}{|}}{C}}+\cdot CF_3$$

The hydroxy radical from the previous step likely combines with trifluoromethyl radical to form a trifluoromethanol (CF$_3$OH) which is unstable and results in the production of COF$_2$ and hydrogen fluoride (HF).[42]

Each occurrence of photo-oxidation and β-scission of the PFPE polymer results in loss of COF$_2$ which is supported by the reduction of fluorocarbon species in the XPS. Data in the F 1s
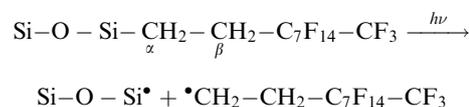
available carbon species for photo-oxidative degradation. The silanol functional group, Fig. 6, of FAS-17 will strongly adhere to the glass by first hydrolysing to form Si–OH bonds (I), and then condensing to create strong Si–O–Si bonds (II) between FAS-17 monomers, and finally forming covalent bonds with the glass Si–OH bonds forming strong Si–O–Si bonds (III) at the substrate surface.[44]

$$\textbf{(I)} \quad H_3C-O-\underset{\underset{H_3C-O}{|}}{\overset{\overset{H_3C-O}{|}}{Si}}-C_2H_4-C_7F_{14}-CF_3 \ + \ 3H_2O \longrightarrow HO-\underset{\underset{HO}{|}}{\overset{\overset{HO}{|}}{Si}}-C_2H_4-C_7F_{14}-CF_3 \ + \ 3CH_3OH$$

$$\textbf{(II)} \quad 2\left[HO-\underset{\underset{HO}{|}}{\overset{\overset{HO}{|}}{Si}}-C_2H_4-C_7F_{14}-CF_3 \right] \longrightarrow \begin{array}{c} HO \\ | \\ HO-Si-C_2H_4-C_7F_{14}-CF_3 \\ | \\ O \\ | \\ HO-Si-C_2H_4-C_7F_{14}-CF_3 \\ | \\ HO \end{array} \ + \ H_2O$$

$$\textbf{(III)} \quad \begin{array}{c} HO \\ | \\ HO-Si-C_2H_4-C_7F_{14}-CF_3 \\ | \\ O \\ | \\ HO-Si-C_2H_4-C_7F_{14}-CF_3 \\ | \\ HO \end{array} \longrightarrow \begin{array}{c} HO \\ | \\ -Si-O-Si-C_2H_4-C_7F_{14}-CF_3 \\ | \\ O \\ | \\ -Si-O-Si-C_2H_4-C_7F_{14}-CF_3 \\ | \\ HO \end{array} \ + \ 2H_2O$$

spectra reveals the C–F at% at 689.0 eV reduces by 20% over 1000 hours whilst in the O 1s spectra C–O peaks at 531.5 eV and OCF$_x$ peaks at 535.5 eV decrease by 40 and 20 at% respectively, Fig. 5c and d. The loss of fluorocarbons from the surface coupled with the presence of polar organic species such as C=O is the cause for the drop in hydrophobic performance of the coating. Minimising the availability of the central carbon species to electronegative free radicals would increase the UV durability of the coating. This can be achieved by reducing the amount of side chains on the PFPE polymer to a straight linear chain structure with no side chain structure ((–CF$_2$–CF$_2$–O–)$_m$-(–CF$_2$–O–)$_n$) which reportedly results in stronger overall bonds and higher resistance to radiation.[43]

3.2.2. FAS-17 degradation mechanisms. Compared to the PFPE coating, the FAS-17 coating is much thinner with more

The strong silica (SiO$_2$) bond and strong fluorocarbon bonds in the central chain leave the central ethyl group available for photo-oxidation.[45] Photo-induced scission will occur at a susceptible carbon atoms in the chain, either α and β, it is difficult to determine the initial site of photo-induced scission, however data from the XPS suggests that degradation occurs at the α carbon due to 75% reduction in CC/CH signal at 284.8 eV between 0 and 250 hours, as shown in Fig. 6a and b, indicating majority loss of methyl groups. The homolysis of the Si–C bond results in the formation of radical silica and fluoroalkyl species.
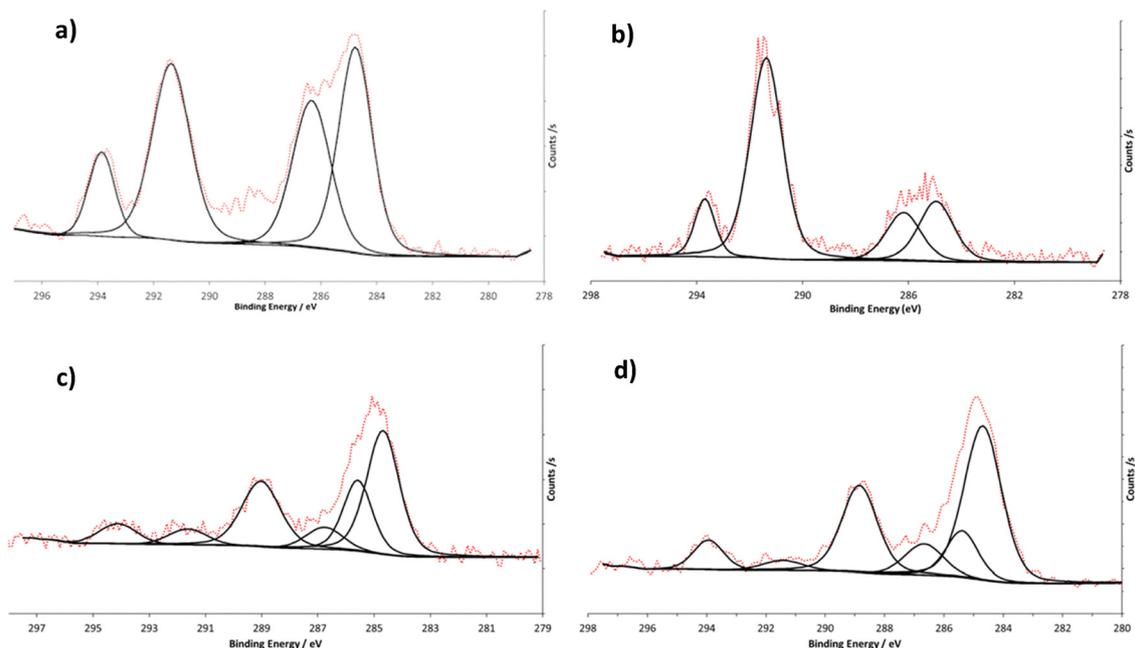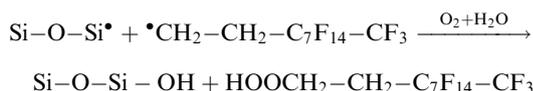
$$Si-O-Si-\underset{\alpha}{CH_2}-\underset{\beta}{CH_2}-C_7F_{14}-CF_3 \xrightarrow{h\nu}$$

$$Si-O-Si^\bullet + {}^\bullet CH_2-CH_2-C_7F_{14}-CF_3$$

Fig. 6 High resolution XPS spectra for FAS-17 coated samples over 1000 hours of UV exposure. (a) C 1s spectra after deposition, (b) C 1s spectra after 250 hours, (c) C 1s spectra after 750 hours, (d) C 1s spectra after 1000 hours.

The presence of O_2 and H_2O in the atmosphere will interact the radical species to form Si–OH on the surface of the glass and a polymer hydroperoxide species (–OOH).

$$Si-O-Si^{\bullet} + {}^{\bullet}CH_2-CH_2-C_7F_{14}-CF_3 \xrightarrow{O_2+H_2O}$$

$$Si-O-Si-OH + HOOCH_2-CH_2-C_7F_{14}-CF_3$$

Whilst it is likely the hydroperoxide species will continue to degrade similar to that of PFPE, with the hydroperoxide species undergoing photo-oxidation to produce a carboxylic acid by direct oxidation or an oxidation involving the formation of aldehydes, the XPS reveals there are no C=O peaks at 288.5 eV until 750 hours of accelerated UV exposure (Fig. 6c). This indicates that once the photo-induced scission occurs the fluorocarbon species is completely removed from the surface, and any carbonyl groups on the surface occur once the majority of fluorinated groups are ejected from the surface and adventitious carbon can be adsorbed onto the glass substrate (Fig. 6d).

$$HO-OCH_2-CH_2-C_7F_{14}-CF_3 \xrightarrow{h\nu}$$

$$O=CH-CH_2-C_7F_{14}-CF_3 + H_2O$$
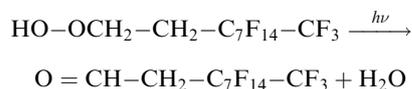
Evidence of this was supported by the F 1s and Si 2p XPS spectra. In the F 1s spectra, surface C–F at 689.0 eV drops from 44.2 at% to 4.6 at%, whilst the Si 2p peak for organic silicon (CH–Si) at 102.7 eV decreases from 9 at% to 0 at%, and instead, a new signal is detected at 103.5 eV corresponding to silica (SiO_2) which would be detected from the glass substrate.

Finally, to indicate the removal of FAS-17 coating, XPS survey scans detected the presence of Na 1s, Mg 1s, and Ca 2p in quantities greater than 1.5 at% indicating these metallic signals are originating from the glass composition rather than external surface contamination.

Due to the thinness of the FAS-17 coating ($<$200 nm), the benefits of the lower refractive index are not as pronounced as indicated by the marginal WAT improvements. The thinness of the coating proved to have detrimental effects as an anti-soiling coating as susceptible elements within the chain were readily targeted by radiative energy leading to complete removal of the coating. A thicker coating would provide additional benefit as a hydrophobic coating as photo-oxidation only occurs at the top most surface of a fluoropolymer,[40] and a thicker coating would have longer chains to maintain coating performance.

3.3. DH accelerated exposure

After 1000 hours of exposure in the accelerated DH weathering chamber each of the coatings exhibit a loss of optical transmittance, Fig. 7. The PFPE coating once again started with the highest WAT values of 92.6 T%, however, after 500 hours the transmittance decreased by an absolute ~1.1% and was outperformed by the FAS-17 coating. By 1000 hours, the PFPE coating performed the worst out of the samples with a total absolute loss of ~2.3% decreasing to 90.3 T%. The FAS-17 coating degraded steadily, reducing from 92.4 T% to 91.6 T% indicating a slower degradation to DH compared to the PFPE coating. The glass control exhibited comparable loss of performance to the FAS-17 coating decreasing WAT by an absolute 0.9 T% from 91.9 T% to 91 T%. This reduction in performance highlights that the FAS-17 hydrophobic coating does provide
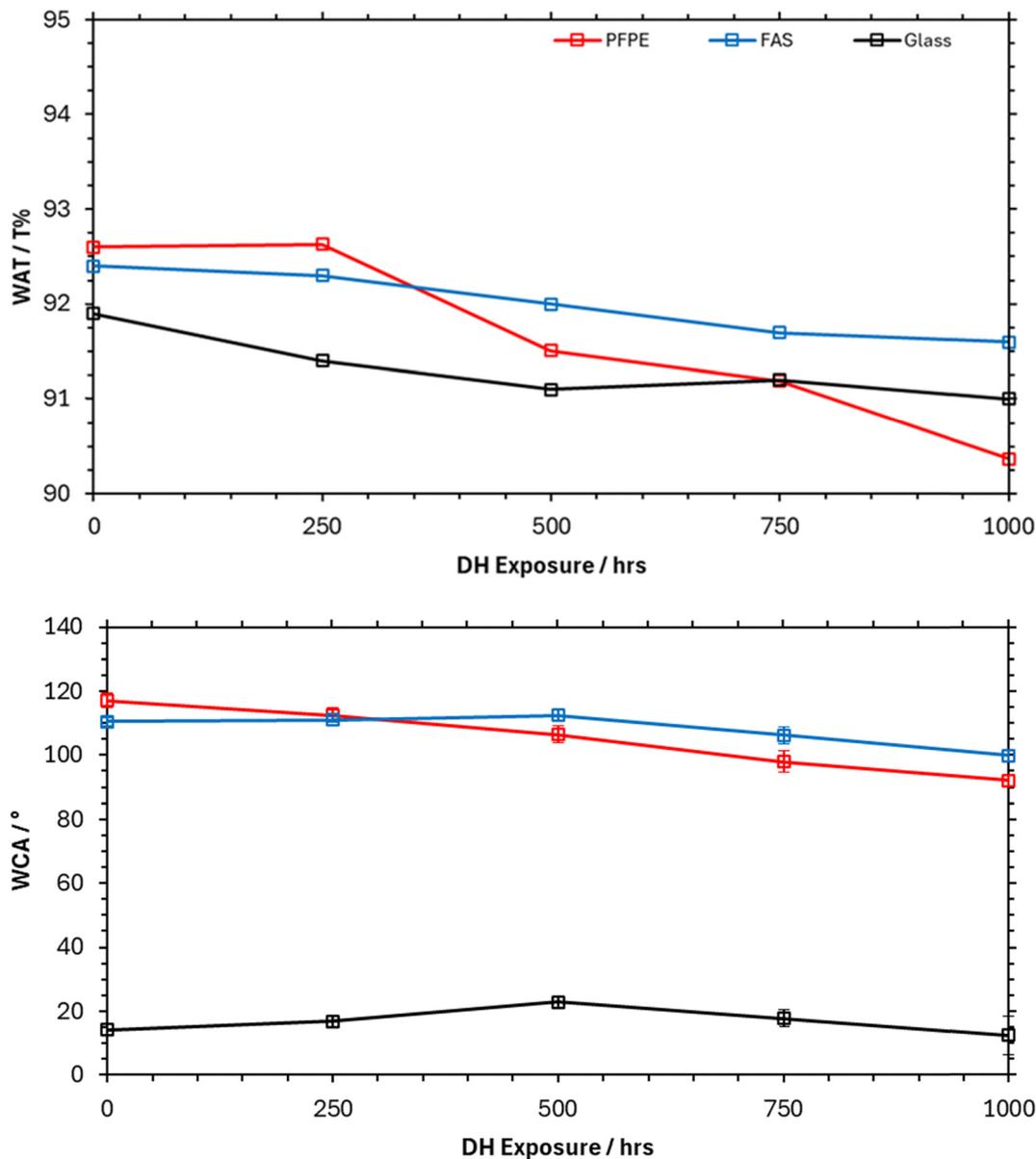
Fig. 7 (top) Weighted average transmission and (bottom) water contact angle of hydrophobic, anti-soiling coatings after 1000 hours of accelerated DH exposure compared to a soda–lime glass control.

benefits to the cover glass in hot and damp environments as the optical transmittance of the coating starts at a higher value and decreases at a slower rate.
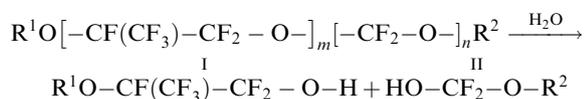
As opposed to the UV accelerated exposure, both hydrophobic coatings retained their hydrophobic properties over the 1000 hours of DH exposure. The PFPE coating exhibited the greatest drop in hydrophobic performance with the WCA decreasing from 117.0° to 92.0°. The FAS-17 coating maintained higher hydrophobicity with the WCA decreasing by ∼10° from 110.6° to 99.8° over 1000 hours exhibiting high performance. The retained hydrophobic properties of the coatings coupled with increased WAT during testing indicates the advantages a hydrophobic coating can apply to PV module cover glass, as well as their resistance to degradation in these environments.

Compared to the UV testing, the glass control substrate exhibited a stable hydrophilic property, this is due to adhered organic species being susceptible to the higher temperature and presence of nucleophilic water species. Nucleophilic species would promote reaction and removal of volatile species from the surface, thereby continuously 'cleaning' the glass, leaving it unaltered due to its extremely low water solubility. This is supported by the XPS data where after 1000 hours of DH exposure, the glass survey data detects <10 at% of surface carbon with a strong 2 : 1 stoichiometric ratio Si 2p at 103.5 eV to O 1s at 532.5 eV attributed to SiO_2.
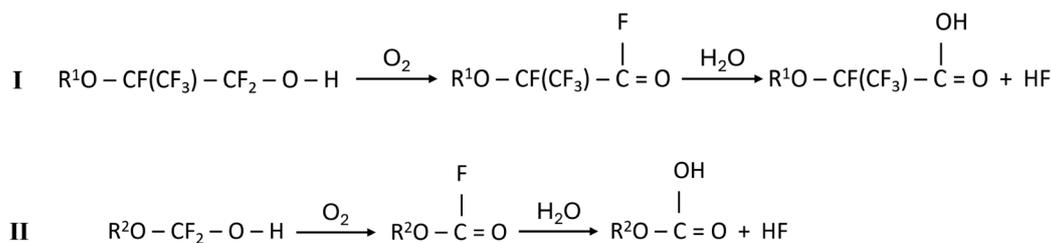
3.3.1. PFPE degradation mechanisms. Due to the low polarity of C–F bonds, fluoropolymers are extremely resistant to degradation *via* hydrolysis.[38] However, this is most prevalent

in linear fluoropolymers with repeating CF_2 units, whereas ether bonds form partial charges (δ^+) on the central secondary carbon atoms leaving them available for nucleophilic attack.[46] The δ^+ carbon atoms would form the site of the hydrolytic attack leading to chain scission and removal of surface fluorocarbons.[47]

$$R^1O\left[-CF(CF_3)-CF_2-O-\right]_m\left[-CF_2-O-\right]_n R^2 \xrightarrow{H_2O}$$
$$\underset{I}{R^1O-CF(CF_3)-CF_2-O-H} + \underset{II}{HO-CF_2-O-R^2}$$

Homolysis of the C–O–C ether bond would result in the formation of 2 fluoroalcohol species (I) and (II). Due to the instability of these intermediate species, and the presence of oxygen within the DH chamber, the flouroalochol will undergo alcohol oxidation, to an intermediate aldehyde species followed by subsequent oxidation into a fluorinated carboxylic acid species.[48]

by 1000 hours, Fig. 8c. This indicates that hydrolyzation begins to occur after 250 hours of DH exposure, with the initial formation of fluoraldehyde species producing a greater signal of C=O bonds at 288.1 eV with increased/complete hydrolyzation occurring later.

Compared to UV exposure, PFPE losses C–F material from the surface at a similar rate with a 20% reduction in C–F material over 1000 hours. However, due to the intermediate species and final products produced by hydrolyzation, a greater amount of polar organic species are present on the surface. XPS of the C 1s spectra indicates a 300% increase in surface C–O at 286.4 eV from 0.6 at% to 1.8 at% whilst C=O at 288.4 eV increases from 0 at% to 1.8 at%. The fluoraldehyde and fluorinated carboxylic species would have a greater reduction on the WCA performance of the coating. The oxygen in the central C–O–C introduces weakness into potential anti-soiling, hydrophobic coatings. To improve coating development,

$$\mathbf{I}\quad R^1O-CF(CF_3)-CF_2-O-H \xrightarrow{O_2} R^1O-CF(CF_3)-\underset{\underset{F}{|}}{C}=O \xrightarrow{H_2O} R^1O-CF(CF_3)-\underset{\underset{OH}{|}}{C}=O \ +\ HF$$

$$\mathbf{II}\quad R^2O-CF_2-O-H \xrightarrow{O_2} R^2O-\underset{\underset{F}{|}}{C}=O \xrightarrow{H_2O} R^2O-\underset{\underset{OH}{|}}{C}=O \ +\ HF$$

The rate of hydrolyzation is linked to the ratio of C–O to C=O which changes from 1:0 after deposition, Fig. 8a, to 1:1.27 ratio after 250 hours Fig. 8b, before decreasing to 1:1

non-oxygenated fluorinated species should be considered to improve both the hydrolysis resistance of the coating and its resistance to UV radiation.
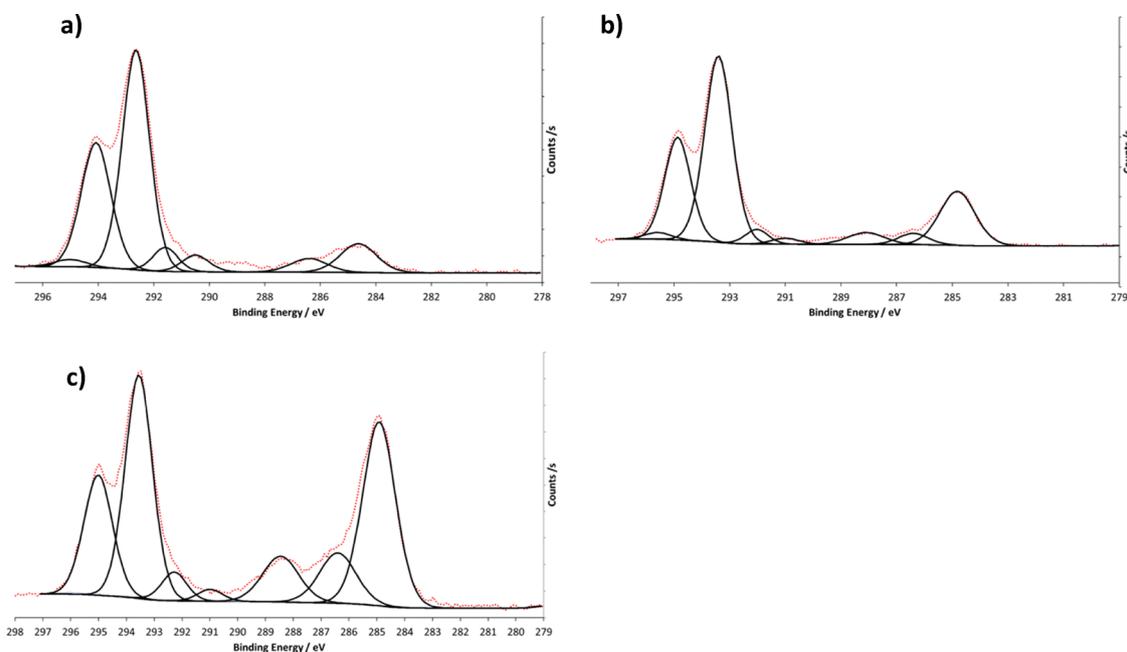

Fig. 8 High resolution XPS spectra for PFPE coated samples over 1000 hours of DH exposure. (a) C 1s spectra after deposition, (b) C 1s spectra after 250 hours, (c) C 1s spectra after 1000 hours.
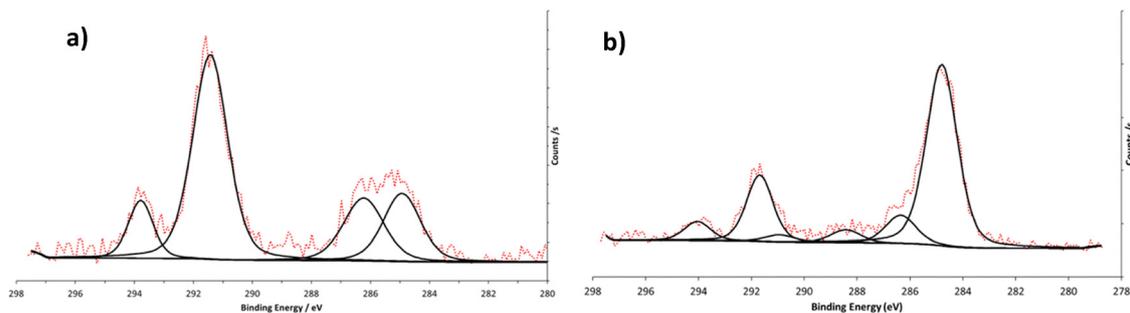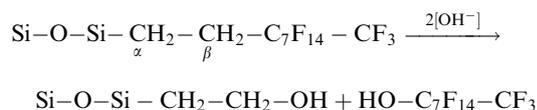
Fig. 9 High resolution XPS spectra for FAS-17 coated samples over 1000 hours of DH exposure. (a) C 1s spectra after deposition, (b) C 1s spectra after 1000 hours.

3.3.2. FAS-17 degradation mechanisms. The FAS-17 coating exhibited a much greater resistance to hydrolysis compared to PFPE. The low total polarity of the CF_2 chains form a shield to decelerate the interaction of nucleophiles on the central carbon chain. Total surface F 1s content remained above 35 at% after 1000 hours of DH exposure, with a small increase in Si 2p and O 1s signal of 3 at% and 6 at% respectively. Some degradation did occur as C–F species were removed from the surface with a reduction of 10 at%, however this had little negative effect on the hydrophobicity of the coating, Fig. 9b.

The strong SiO_2 bond between the FAS-17 and the glass was formed by hydrolysis and subsequent condensation indicating a reverse reaction could be feasible as a degradation mechanism, but lack of Si–OH bonds at 100.0 eV (ref. 49) in the Si 2p XPS spectra indicate this was not the case. Therefore, between the two susceptible secondary carbons, α and β, nucleophilic species will attack the β carbon.

$$Si-O-Si-\underset{\alpha}{CH_2}-\underset{\beta}{CH_2}-C_7F_{14}-CF_3 \xrightarrow{2[OH^-]}$$

$$Si-O-Si-CH_2-CH_2-OH + HO-C_7F_{14}-CF_3$$

These reactions are slow at ambient temperatures, but the increased temperature of the DH chamber accelerates this mode of degradation. The scission of the C–C chain results in the formation of radical hydroxy functional groups at the end of the constituent chains. These hydroxy groups are susceptible to further oxidation and hydrolysis resulting in the formation of carboxylic acid species. However, the rate of hydrolyzation in FAS-17 is much slower as the ratio of C–O to C=O in the C 1s XPS spectra is which changes from 1:0 after deposition, and 2:1 ratio after 1000 hours indicating resistance to the formation of an fluoraldehyde intermediate species.

$$CF_3-C_6F_{12}-CF_2-O-H \xrightarrow{O_2} CF_3-C_6F_{12}-\overset{\overset{\textstyle F}{\textstyle |}}{C}=O$$
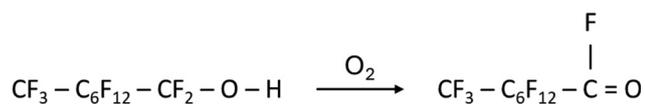
Additional data to support the scission at the β carbon is the presence of COF bond at 290.9 eV after 500 hours, Fig. 9b. Scission occurring at that Si–C bond would not produce the COF signal as hydrolysis would occur at the end of the polymer chain on the available methyl group. Subsequently, rather than chemical degradation of the Si–C bond, there is evidence of the higher kinetic energy of the hot water molecules disrupting the interfacial bond between the FAS-17 and glass, resulting in coating detachment. This is evidenced by the detection of a SiO_2 signal in the Si 2p peak at 103.5 eV from 500 hours onwards, resulting in a surface Si 2p increase of 6.8 at% to ~13.5 at% after 1000 hours. Additionally, the 1000-hour sample survey scan reveals the presence of Na, Mg and Ca which are present from the glass substrate.

The resistance to hydrolysis exhibited by FAS-17 indicates the importance of a central carbon containing chain with no oxygen that could act as a site of nucleophilic attack. CF_2 and CF_3 bonds exhibit great resistance to hydrolysis whilst improving the hydrophobic properties of the coating. Coating thickness is also important as thin coatings are susceptible to physical coating removal, thicker coatings (>1 μm) or multi-layer coatings would provide greater resistance to hydrolysis however coating development must consider the t impact of thicker coatings on optical performance.

Conclusions

Soiling is a serious problem for solar utility asset management. By attenuating the light reaching the PV absorber, it reduces the number of carriers generated and the current density leading to a loss in overall power generation. Cleaning a solar utility is costly and reduces the financial rate of return. Although the losses will depend on the precise location of the assets, the basic problem is the low surface energy of the glass, or the anti-reflection coating applied to the glass. Both plain glass and coated glass are hydrophilic, meaning that they have high surface free energy. This means that these surfaces will tend to adhere to soiling. A hydrophobic coating would be advantageous, because the module surface would then have low surface free energy, and it would adhere less well to soiling. This would reduce the amount of soiling retained by the surface and it would also make the surface much easier to clean.

The same problem has been addressed by spectacle lens manufacturers especially for lenses with an anti-reflection coating. Hydrophobic coatings are now used ubiquitously on ophthalmic lenses. These coatings are very thin to avoid

making a noticeable contribution to the destructive interference of the underlying anti-reflection coatings. PFPE and FAS-17 hydrophobic polymers are commonly used for this application. These coatings are also effective for anti-soiling of solar modules providing proof of principle that the use of hydrophobic coatings would increase the power output of solar utilities. However, although these coatings are effective, they degrade after a short time in outdoor conditions and gradually become hydrophilic. The vastly increased UV and humidity exposure when the coatings are exposed outdoors 24/7 is the major cause of the degradation. A hydrophobic coating is required that does not suffer the degradation observed in PFPE and FAS-17. Here we have examined the precise mechanisms that cause the degradation to identify chemical structural weaknesses that must be avoided in a hydrophobic coating designed specifically for use on solar modules.

PFPE and FAS-17 hydrophobic coatings were deposited onto soda–lime glass substrates and exposed to accelerated weathering conditions; UV and DH and compared to regular soda–lime glass as a control. During UV accelerated testing the PFPE and FAS-17 coatings were found to undergo photo-oxidation after 1000 hours of exposure, whilst during DH accelerated testing scission would occur in the PFPE coating due to hydrolysis occurring at the central ether bond. The FAS-17 coating exhibited greater resistance to degradation during DH exposure.

The analysis showed that the weakness of the PFPE coating was oxygen present in the central carbon chain. During UV exposure or DH exposure, the central ether bond acted as the site for photo-oxidation and nucleophilic attack. Additionally, the existence of branch chains increases the availability of central carbon chains to substitution.

The FAS-17 coating failed after 1000 hours of UV exposure due to β scission of the fluorocarbons chain from the silanol group resulting in large amounts of fluorocarbon loss and therefore a degradation of its hydrophobic properties. The FAS-17 coating highlighted the importance of maintaining fluorocarbon bonds in the hydrophobic coating during DH testing. Thinning of the coating was also observed which would also reduce the lifetime of the coating in the field.

The design of improved anti-soiling coatings should therefore focus on non-oxygenated chemical compounds that have a symmetrical polarity, and a linear carbon chain. Additionally, coating thickness is a factor that must be balanced when developing a hydrophobic, anti-soiling coating, with thicker coatings providing greater mechanical and chemical durability at the potential cost of optical properties. Ethylene tetrafluoroethylene (ETFE), fluorinated ethylene propylene (FEP), and Polyvinyl fluoride (PVF) are such polymers that do not feature oxygen in the central carbon chain, have low refractive indices, exhibit hydrophobic properties, and are chemically stable, therefore are promising candidates for future, durable, hydrophobic, anti-soiling coatings.

Author contributions

L. O. Jones – formal analysis, investigation, methodology, visualization, writing (original draft). A. M. Law – investigation,

validation, writing (review & editing). W. Critchlow – project administration, resources, supervision, validation. M. J. Walls – conceptualization, funding acquisition, project administration, resources, supervision, validation, writing (review & editing).

Conflicts of interest

There are no conflicts to declare.

Data availability

Data for this article are available at The Open Science Framework Repository at [**https://osf.io/wh4p9/?view_only=896466 faf7dc446daaf6e3f78295678a**, doi: **https://doi.org/10.17605/OSF. IO/WH4P9**].

Acknowledgements

References

1 C. Kost, J. N. Mayer, J. Thomsen, N. Hartmann, C. Senkpiel, S. Philipps, S. Nold, S. Lude, N. Saad and T. Schlegl, *Levelized cost of electricity - renewable energy technologies*, Fraunhofer ISE, Freiburg/Brsg, 2013.

2 K. Osmani, A. Haddad, T. Lemenand, B. Castanier and M. Ramadan, *Sci. Total Environ.*, 2020, **746**, 141753.

3 L. Micheli, E. F. Fernandez, J. T. Aguilera and F. Almonacid, *Energy*, 2021, **215**, 119018.

4 J. G. Bessa, L. Micheli, F. Almonacid and E. F. Fernández, *Iscience.*, 2021, **24**(3), 102165.

5 P. Borah, L. Micheli and N. Sarmah, *Sustainability*, 2023, **15**, 16669.

6 K. K. Ilse, B. W. Figgis, V. Naumann, C. Hagendorf and J. Bagdahn, *Renewable Sustainable Energy Rev.*, 2018, **98**, 239–254.

7 C. Sanz-Saiz, J. Polo, N. Martin-Chivelet and M. del Carmen Alonso-García, *J. Cleaner Prod.*, 2022, **332**, 130041.

8 M. Mahamudul Hasan Mithhu, T. Ahmed Rima and M. Ryyan Khan, *Appl. Energy*, 2021, **285**, 116436.

9 S. K. Yadav, N. M. Kumar, G. Aritra, B. Usha and S. S. Chopra, *Sol. Energy*, 2022, **242**, 119–129.

10 Z. Hao, H. Lu and W. Zhao, *Renewable Energy*, 2024, **237**, 121614.

11 B. Figgis and B. Brophy, Conference Proceedings PV-Days Halle, **20**, 1–9. 2015.

12 L. Kazmerski, L. Diniz, C. B. Maia, M. M. Viana, S. C. Costa, P. P. Brito, C. D. Campos, L. V. Macheto Neto, S. de Morais Hanriot and L. R. de Oliveira Cruz, *IEEE J. Photovolt.*, 2016, **6**, 719–729.

13 L. O. Jones, A. M. Law, G. Critchlow and J. M. Walls, Presented in 2023 IEEE 50th Photovoltaic Specialist Conference (PVSC), San Juan, June 2024.

14 M. I. Hossain, A. Ali, V. B. Benito, B. Figgis and B. Aissa, *Materials*, 2022, **15**, 7139.

15 Z. S. Huang, C. Shen, L. Fan, X. Ye, X. Shi, H. Li, Y. Zhang, Y. Lai and Y. Y. Quan, *Sol. Energy Mater. Sol. Cells*, 2021, **225**, 111053.

16 H. Lu, B. He and W. Zhao, *Sol. Energy*, 2023, **249**, 725–733.

17 A. Aldawoud, A. Aldawoud, Y. Aryanfar, M. El Haj Assad, S. Sharma and R. Alayi, *Int. J. Low-Carbon Technol.*, 2022, **17**, 919–930.

18 F. Lisco, F. Bukhari, S. Ulicna, K. Isbilir, K. L. Barth, A. Taylor and J. M. Walls, *Energies*, 2020, **13**(2), 299.

19 L. O. Jones, A. M. Law, G. Critchlow and J. M. Walls, *Presented in 2022 IEEE 49th Photovoltaics Specialists Conference (PVSC)*, Philadelphia, June 2022.

20 D. Adak, R. Bhattacharyya and H. C. Barshilia, *Renewable Sustainable Energy Rev.*, 2022, **159**, 112145.

21 J. Qin and H. Lu, *Environ. Sci. Pollut. Res.*, 2023, **30**, 91591–91616.

22 N. Gupta, M. V. Kavya, Y. R. G. Singh, J. Jyothi and H. C. Barshilia, *J. Appl. Phys.*, 2013, **114**, 164307.

23 P. Fabbri, M. Messori, F. Pilati, R. Taurino, C. Tonelli and M. Toselli, *Adv. Polym. Technol.*, 2007, **26**, 182–190.

24 N. Satyanarayana and S. K. Sinha, *J. Phys. D: Appl. Phys.*, 2005, **38**, 3512.

25 S. A. Tayel, A. E. A. El-Maaty, E. M. Mostafa and Y. F. Elsaadawi, *Sci. Rep.*, 2022, **12**, 21236.

26 L. O. Jones, F. Bukhari, G. Critchlow and J. M. Walls, Presented in 2021 IEEE 48th Photovoltaic Specialists Conference (PVSC), June 2021.

27 G. C. Oehler, F. Lisco, F. Bukhari, S. Ulicná, B. Strauss, K. L. Barth and J. M. Walls, *Energies*, 2020, **13**, 299.

28 M. Aghaei, A. Fairbrother, A. Gok, S. Ahmed, S. Kazim, K. Lobato, G. Oreski, A. Reinders, J. Schmitz, M. Theelen, P. Yilmaz and J. Kettle, *Renewable Sustainable Energy Rev.*, 2022, **159**, 112160.

29 A. Fernandez-Solas, L. Micheli, F. Almonacid and E. F. Fernandez, *Renewable Sustainable Energy Rev.*, 2021, **141**, 110782.

30 D. E. Mansour, C. Barretta, L. P. Bauermann, G. Oreski, A. Scheuler, D. Philipp and P. Gebhardt, *Sustainability*, 2020, **12**, 5208.

31 E. Yousif and R. Haddad, *SpringerPlus*, 2013, **2**, 1–32.

32 L. Sørensen, A. S. Groven, I. A. Hovsbakken, O. Del Puerto, D. F. Kraus, A. Sarno and A. M. Booth, *Sci. Total Environ*, 2021, **755**, 143170.

33 N. Grassie and G. Scott, *Polym. Anal., Degrad., Stab.*, 1985, 68–85.

34 B. Gewert, M. M. Plassmann and M. Macleod, *Environ. Sci.: Processes Impacts*, 2015, **17**, 1513–1521.

35 P. Kirsch, *Modern fluoroorganic chemistry: synthesis, reactivity, applications*, John Wiley & Sons, 2013.

36 K. Woord, *Macromol. Symp.*, 2002, **187**, 1.

37 National Institute of Standards and Technology, NIST X-ray Photoelectron Spectroscopy Database, NIST Standard Reference Database Number 20, 2000. [Online]. Available: **https://srdata.nist.gov/xps/**. [Accessed April 2024].

38 D. O'Hagan, *Chem. Soc. Rev.*, 2008, **37**, 308–319.

39 J.-L. Gardette, B. Mailhot-Jensen, F. Prosada, A. Rivaton and C. Maitre, *Macromol. Symp.*, 1999, **143**, 95–109.

40 W. Burger, K. Lunkwitz, G. Pompe, A. Petr and D. Jehnichen, *J. Appl. Polym. Sci.*, 1993, **48**, 1973–1985.

41 J. Schiers, G. Camino, L. Costa, C. Tonelli, S. Turri and M. Scicchitano, *Polym. Degrad. Stab.*, 1996, **56**, 239–253.

42 K. Seppelt, *Angew. Chem.*, 1977, **16**, 322–323.

43 N. Tadokoro, S. Pannakarn, J. Wisuthtatip, S. Kunchoo, V. Parnich, K. Takashiba, K. Shimizu and H. Higuchi, *J. Surf. Anal.*, 2011, **17**, 190–193.

44 H. Fu, S. Liu, L. Yi, H. Jiang, C. Li and Y. Chen, *Materials*, 2020, **13**, 1642.

45 H. Li, L. Chen and W. Zhang, *ACS Sustainable Chem. Eng.*, 2022, **10**, 4642–4649.

46 X. Chen, K. Inayoshi, H. Zhang, N. Koga, K. Fukuzawa, S. Itoh and N. Azuma, *Tribol. Int.*, 2023, **187**, 108674.

47 I. Boullier, S. Esnouf and A. Le Moel, *J. Polym. Sci., Part B:Polym. Phys.*, 2003, **41**, 1509–1517.

48 N. Ohno, K. Sonoda, H. Tsuchida and S. Obara, *Tribol. Trans.*, 2011, **54**, 859–866.

49 A. U. Alam, M. M. Howlader and M. J. Deen, *ECS J. Solid State Sci. Technol.*, 2013, **2**, 515–523.